ACS APPLIED MATERIALS & INTERFACES

Research Article

www.acsami.org

Mesoporous Mn- and La-Doped Cerium Oxide/Cobalt Oxide Mixed Metal Catalysts for Methane Oxidation

Susan M. Vickers,[†] Rahman Gholami,[‡] Kevin J. Smith,*[,‡] and Mark J. MacLachlan*[,†]

[†]Department of Chemistry, University of British Columbia, 2036 Main Mall, Vancouver, British Columbia, Canada V6T 1Z1

[‡]Department of Chemical and Biological Engineering, University of British Columbia, 2360 East Mall, Vancouver, British Columbia, Canada V6T 1Z3

Supporting Information

ABSTRACT: New precious-metal-free mesoporous materials were investigated as catalysts for the complete oxidation of methane to carbon dioxide. Mesoporous cobalt oxide was first synthesized using KIT-6 mesoporous silica as a hard template. After removal of the silica, the cobalt oxide was itself used as a hard template to construct cerium oxide/cobalt oxide composite materials. Furthermore, cerium oxide/cobalt oxide composite materials doped with manganese and lanthanum were also prepared. All of the new composite materials retained the hierarchical long-range order of the original KIT-6 template. Temperature-programmed oxidation measurements showed that these cerium oxide/cobalt oxide and doped cerium oxide/cobalt oxide materials are effective catalysts for the total oxidation of methane, with a light-off temperature ($T_{50\%}$) of ~400 °C observed for all of the nanostructured materials.

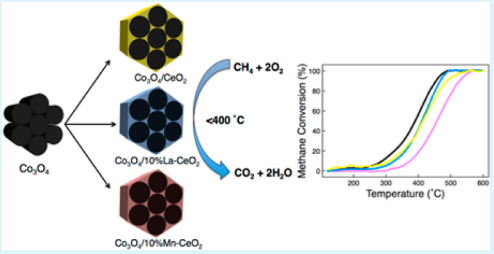

KEYWORDS: *methane oxidation, mesoporous, cobalt oxide, cerium oxide, KIT-6, hard templating*

INTRODUCTION

Natural gas (mostly methane) produces less CO_2 per unit energy than gasoline or diesel and is thus a possible "green" substitute for these fuels.[1] However, the full potential of natural gas as a fuel for vehicles cannot yet be realized due to the unburned methane expelled in the exhaust. Methane is a significant greenhouse gas with a potency much higher than that of CO_2.[2] The high C−H bond strength (~435 kJ mol^{-1}) and lack of a dipole in methane renders it relatively unreactive compared to other hydrocarbons. Thus, a challenging problem in this field is the development of effective catalysts for the complete oxidation of methane at the low temperatures (less than 500 °C) for application in natural gas vehicle (NGV) engines.[3]

Research into methane oxidation catalysts has largely focused on precious metals, such as platinum and palladium.[3−6] Transition-metal-based catalysts have been investigated as less expensive alternatives to the traditional noble-metal-based catalysts, but none has achieved the necessary high activity at low temperatures. Ceria (CeO_2) has shown promise due to its ability to release and absorb oxygen during alternating redox conditions, and hence to function as an oxygen buffer.[7−9] These characteristics originate from the facile Ce^{3+}/Ce^{4+} redox cycle. Efforts to increase the oxygen storage capacity of ceria by the introduction of cationic dopants have been successful, and ceria-based materials have been prepared with a variety of dopant cations such as $Zr^{3+/4+}$, Hf^{4+}, La^{3+}, Pr^{3+}, and $Mn^{3+/4+}$.[9−13] Compared to undoped ceria, most of these materials show enhancement of both oxygen vacancy concentration and oxygen storage capacity, as well as of redox activities.

Recently, there has been substantial interest in Co−Ce composite oxides as catalysts for the oxidation of CO, N_2O, volatile organic compounds (VOCs), and propene.[14−17] It has been shown that the combination of cerium and cobalt oxides leads to higher activity when compared to the individual component oxides in these reactions due to synergistic effects between the two metal oxides.[18] There have been relatively few studies using Co−Ce composite oxides as catalysts for methane oxidation. Materials prepared by coprecipitation methods have shown high activity but have low surface areas.[19,20] Li et al. successfully prepared a Co_3O_4/CeO_2 composite oxide using a modified citrate sol−gel method to achieve high surface area materials reaching a $T_{50\%}$ as low as 401 °C.[19] However, there is a significant need to explore new Ce−Co−O composite materials with tunable structure and properties beneficial for low-temperature methane oxidation catalysis.

Materials containing mesopores are promising candidates for use as methane oxidation catalysts due to their large surface area, interconnected pores, and controllable pore wall compositions. KIT-6 is a mesoporous silica material with a three-dimensional cubic structure (space group Ia3d) that is synthesized using a block copolymer template.[21] Mesoporous metal oxides can be successfully templated using KIT-6.[22−25] Co_3O_4 templated with KIT-6 shows high activity for CO

Received: March 17, 2015
Accepted: May 12, 2015
Published: May 22, 2015

DOI: 10.1021/acsami.5b02367
ACS Appl. Mater. Interfaces 2015, 7, 11460−11466

oxidation, resulting from the high surface area and open pore system of the material.[26,27] Mesoporous cobalt oxide materials templated by KIT-6 have also shown high activities for various hydrocarbon oxidations.[28−30] To the best of our knowledge, however, these materials have never been evaluated for methane oxidation.

In this study, we describe a straightforward and scalable method to make catalysts based on templating with KIT-6. Cobalt oxide was prepared in the channels of KIT-6 and released after etching of the silica. The mesoporous Co_3O_4 was then used itself to template CeO_2, La-doped CeO_2, and Mn-doped CeO_2 within its pores. These hierarchically organized catalysts show high activity for methane oxidation at low temperature.

EXPERIMENTAL SECTION

All chemicals and solvents were purchased from commercial suppliers and used without further purification. Mesoporous silica, KIT-6, was synthesized according to the established method.[21] *Meso*-Co_3O_4 was synthesized using a procedure similar to that used by Yue et al.[31]

Preparation of Mesoporous Co_3O_4 (*meso*-Co_3O_4). KIT-6 (2.075 g) was ground with $Co(NO_3)_2{\cdot}6H_2O$ (4.016 g, 13.79 mmol) using a pestle and mortar and was then heated to 500 °C at a ramp rate of 1 °C/min in a muffle furnace. The furnace was maintained at 500 °C for 3 h before cooling under ambient conditions. During the slow heating, $Co(NO_3)_2{\cdot}6H_2O$ melts at 55 °C and enters the KIT-6 pores via capillary action before it decomposes to Co_3O_4 at 74 °C. After cooling, the silica was removed by stirring the product in 2 M NaOH for 2 h. The resulting black solid was collected and washed with H_2O (2 × 20 mL) and EtOH (2 × 20 mL) via centrifugation then dried overnight at 70 °C. Yield: 1.233 g. PXRD of the black product showed that it was crystalline Co_3O_4. N_2 adsorption showed a surface area of 97 $m^2\ g^{-1}$ and a type IV isotherm with a hysteresis loop. XPS and EDX confirmed the presence of Co and O and showed only traces of residual Si from the template.

Preparation of *meso*-Co_3O_4/CeO_2 Composite. As-synthesized *meso*-Co_3O_4 (0.400 g, 1.66 mmol) was placed in a Schlenk flask and evacuated for 1 h. $Ce(NO_3)_3{\cdot}6H_2O$ (0.220 g, 0.506 mmol) was dissolved in 5 mL of EtOH then added dropwise via syringe. The sample was then left to dry under vacuum overnight and calcined at 500 °C under air for 5 h. Yield: 0.420 g. PXRD of the black product showed that is was crystalline Co_3O_4 and CeO_2. N_2 adsorption showed a surface area of 68 $m^2\ g^{-1}$ and a type IV isotherm with a hysteresis loop. XPS and EDX confirmed the presence of Co, Ce, and O.

Preparation of *meso*-Co_3O_4/10%La-CeO_2 Composite. As-synthesized *meso*-Co_3O_4 (0.400 g, 1.66 mmol) was placed in a Schlenk flask and evacuated for 1 h. $Ce(NO_3)_3{\cdot}6H_2O$ (0.198 g, 0.469 mmol) and $La(NO_3)_3{\cdot}6H_2O$ (0.022 g, 0.051 mmol) were dissolved in 5 mL of EtOH then added dropwise via syringe. The sample was then left to dry under vacuum overnight and calcined at 500 °C under air for 5 h. Yield: 0.412 g. PXRD of the black product showed peaks corresponding to crystalline Co_3O_4 and CeO_2. N_2 adsorption showed a surface area of 67 $m^2\ g^{-1}$ and a type IV isotherm with a hysteresis loop. XPS and EDX confirmed the presence of Co, Ce, La and O.

Preparation of *meso*-Co_3O_4/10%Mn-CeO_2 Composite. As-synthesized *meso*-Co_3O_4 (0.400 g, 1.66 mmol) was placed in a Schlenk flask and evacuated for 1 h. $Ce(NO_3)_3{\cdot}6H_2O$ (0.198 g, 0.469 mmol) and $Mn(NO_3)_2{\cdot}4H_2O$ (0.013 g, 0.051 mmol) were dissolved in 5 mL of EtOH and then added dropwise via syringe. The sample was then left to dry under vacuum overnight and calcined at 500 °C under air for 5 h. Yield: 0.432 g. PXRD of the black product showed peaks corresponding to crystalline Co_3O_4 and CeO_2. N_2 adsorption showed a surface area of 55 $m^2\ g^{-1}$ and a type IV isotherm with a hysteresis loop. XPS and EDX confirmed the presence of Co, Ce, Mn and O.

CHARACTERIZATION

Powder X-ray diffraction (PXRD) data were recorded on a Bruker D8 Advance X-ray diffractometer in the Bragg−Brentano configuration, using Cu Kα radiation at 40 kV, 40 mA. Crystallite size was estimated from the broadening of the (440) peak for Co_3O_4 and the (111) peak for CeO_2 using the Scherrer equation. Transmission electron microscopy (TEM) images were collected on a Hitachi H7600 electron microscope operating at an accelerating voltage of 100 kV. Energy dispersive X-ray analysis (EDX) was collected on a Hitachi S-2600N variable pressure scanning electron microscope (SEM) equipped with an X-ray detector coupled to Quartz Imaging Systems Xone software. X-ray photoelectron spectroscopy (XPS) was carried out on a Leybold Max200 spectrometer using an aluminum Kα X-ray source for samples containing Mn and a magnesium Kα X-ray source for all other samples, operating at a base pressure of 1×10^{-9} Torr. Initial survey scans were acquired with a pass energy of 192 eV, while higher resolution scans were acquired with a pass energy of 48 eV. XPS spectra were deconvoluted using the XPSPEAK program by curve fitting with a mixed Gaussian−Lorentzian function after the Shirley type background subtraction. Gas adsorption studies were performed using a Micromeritics Accelerated Surface Area and Porosity (ASAP) 2020 system.

Methane Oxidation Testing. Temperature-programmed CH_4 oxidation (TPO) was used to evaluate the activities of the prepared catalysts. The TPO setup consisted of a stainless steel fixed-bed microreactor (length = 4.5 cm; i.d. = 0.7 cm) placed inside an electric tube furnace with PID temperature control. Two thermocouples (K-type), placed coaxially in the reactor, measured the temperature at the top and bottom of the catalyst bed. Flow rates of CH_4 (0.76% (v/v) CH_4/Ar, Praxair, certified purity), O_2 (Praxair, UHP), Ar (Praxair, UHP), and He (Praxair, UHP) were set using electric mass flow controllers (Brooks 5850 TR) and mixed to yield a feed gas of 1000 ppmv CH_4, 20% (v/v) O_2, balance He/Ar at a total feed gas flow rate of 300 mL (STP) min^{-1} (WHSV 180 000 cm^3 (STP) $g^{-1}\ h^{-1}$). The feed gas was preheated to 100 °C using a separate furnace before entering the reactor. The catalyst (0.1000 g; 90−354 μm) was diluted four times (v/v) with inert SiC pellets (90−354 μm) to ensure isothermal reactor operation. The diluted catalyst was flushed in 100 cm^3 (STP) min^{-1} flow of Ar at 120 °C for 1 h prior to introducing the reactant gas to the catalyst bed. The reactor temperature was simultaneously increased linearly at 5 °C·min^{-1} from 120 to 600 °C while monitoring the reactor exit gas composition using a VG ProLab quadrupole mass spectrometer (QMS; ThermoFisher Scientific). Mass numbers corresponding to CH_4, CO_2, and He were monitored, and their intensity calibrated using standard gas mixtures (Praxair, certified purity), from which the CH_4 conversion and overall C balance were calculated.

RESULTS AND DISCUSSION

We employed KIT-6, a well-known mesoporous silica, as a template to construct novel hybrid catalytic materials. KIT-6 has large, uniform, easily accessible pores, which make it ideal for use as a template. Nitrogen adsorption measurements of the KIT-6 utilized as a template for *meso*-Co_3O_4 show an H1 hysteresis loop and an average pore size of 7 nm (Figure S1a,b, Supporting Information). The ordered pores, as seen by TEM in Figure S1c (Supporting Information), afford a large surface area of 802 $m^2\ g^{-1}$. The *meso*-Co_3O_4/CeO_2 based catalysts

DOI: 10.1021/acsami.5b02367
ACS Appl. Mater. Interfaces 2015, 7, 11460−11466

Scheme 1. Synthesis of *meso*-Co_3O_4/CeO_2 based Materials Using KIT-6 as a Template

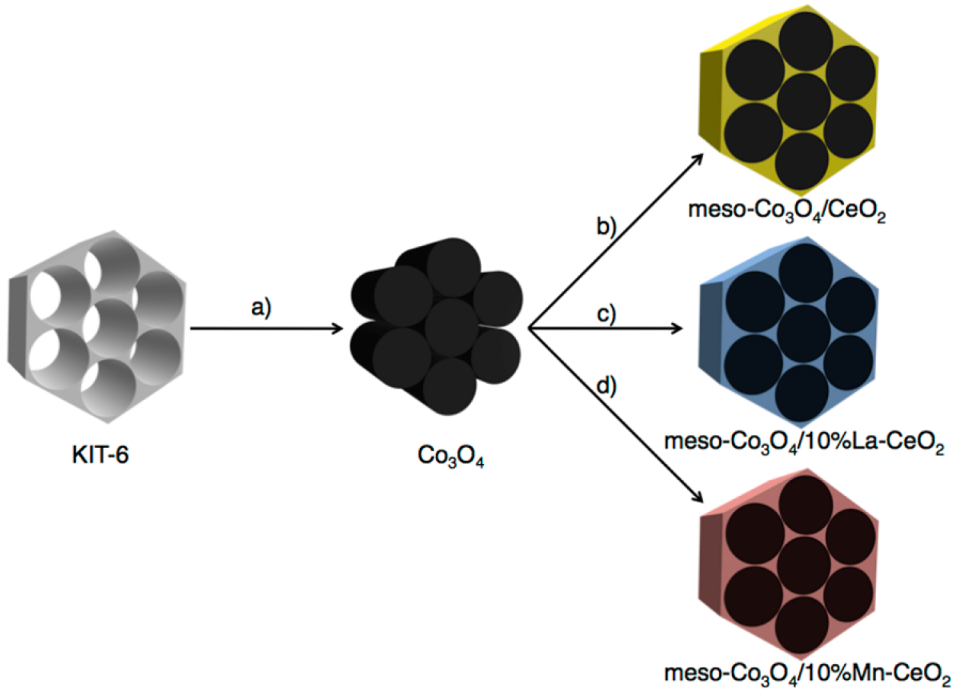

[a]2.075 g of KIT-6 ground with 4.016 g of $Co(NO_3)_2{\cdot}6H_2O$; calcination at 500 °C; etching in 2 M NaOH(aq). [b]0.220 g $Ce(NO_3)_3{\cdot}6H_2O$ in 5 mL EtOH added to 0.400 g *meso*-Co_3O_4 under vacuum; calcination at 500 °C. [c]0.198 g of $Ce(NO_3)_3{\cdot}6H_2O$ and 0.022 g of $La(NO_3)_3{\cdot}6H_2O$ in 5 mL of EtOH added to 0.400 g *meso*-Co_3O_4 under vacuum; calcination at 500 °C. [d]0.198 g of $Ce(NO_3)_3{\cdot}6H_2O$ and 0.013 g of $Mn(NO_3)_2{\cdot}4H_2O$ in 5 mL of EtOH added to 0.400 g *meso*-Co_3O_4 under vacuum; calcination at 500 °C.

templated with KIT-6 were prepared using the route shown in Scheme 1. First, KIT-6 was ground together with cobalt nitrate, then the composite was calcined to give a SiO_2/Co_3O_4 material. Etching of the silica with NaOH(aq) afforded *meso*-Co_3O_4. In a second step, the pores of the *meso*-Co_3O_4 were infiltrated with CeO_2 by dissolving $Ce(NO_3)_3{\cdot}6H_2O$ in EtOH and injecting it into a Schlenk flask containing *meso*-Co_3O_4 under vacuum. Samples were also prepared with CeO_2 enriched with La or Mn using a similar procedure.

PXRD patterns of the calcined catalysts are shown in Figure 1. Diffraction peaks associated with cubic Co_3O_4, space group Fd3m, were observed in all samples. *meso*-Co_3O_4/CeO_2, *meso*-Co_3O_4/10%La-CeO_2 and *meso*-Co_3O_4/10%Mn-CeO_2 also display peaks corresponding to cubic CeO_2 with fluorite-like cubic structure. There are no diffraction peaks of manganese or lanthanum oxide, suggesting that Mn or La has entered into the CeO_2 lattices rather than phase separating into a distinct crystalline oxide phase. We did not observe any shift in the ceria diffraction peaks that one would typically expect for a solid solution, but the peaks did become broader. This is consistent with previous reports of doped ceria.[32] Crystallite sizes were estimated using the Scherrer equation, as shown in Table S1 (Supporting Information).

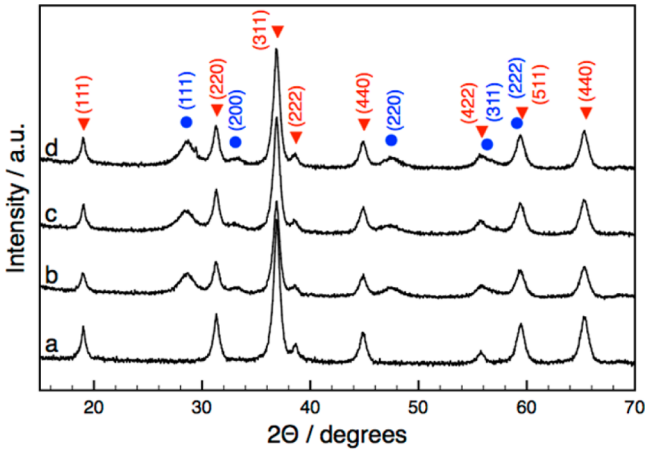

Figure 1. PXRD patterns of (a) *meso*-Co_3O_4, (b) *meso*-Co_3O_4/CeO_2, (c) *meso*-Co_3O_4/10%La-CeO_2, and (d) *meso*-Co_3O_4/10%Mn-CeO_2. (▼) PXRD pattern of *meso*-Co_3O_4 matches JCPDS-78-1969 for Co_3O_4 and (●) the PXRD pattern of CeO_2 matches JCPDS-34-0394.

The as-synthesized materials were examined by nitrogen adsorption/desorption measurements to determine the Brunauer–Emmett–Teller (BET) surface areas and the pore size distributions (Figure 2). The BET surface area of the *meso*-Co_3O_4 decreases from 97 to 68 $m^2\ g^{-1}$ upon addition of $Ce(NO_3)_3{\cdot}6H_2O$ followed by calcination. This relatively small decrease in surface area is due to partial filling of the pores with CeO_2, allowing the surface area to remain relatively high. This is supported by TEM images that show both filled and empty pores (Figure 3d). The confinement of most of the CeO_2 within the *meso*-Co_3O_4 pores is thought to prevent the CeO_2 from any significant sintering upon calcination at 500 °C and allows the Co_3O_4 and CeO_2 to maintain intimate interactions in the solid state, interactions that are expected to be beneficial for catalysis. *meso*-Co_3O_4/10%La-CeO_2 and *meso*-Co_3O_4/10%Mn-CeO_2 have similar surface areas of 67 and 55 $m^2\ g^{-1}$, respectively.

Figure 2 shows N_2 adsorption curves for all of the materials, indicating that they all show typical type IV isotherms with a hysteresis loops defined by IUPAC.[33] This shows that the

DOI: 10.1021/acsami.5b02367
ACS Appl. Mater. Interfaces 2015, 7, 11460–11466

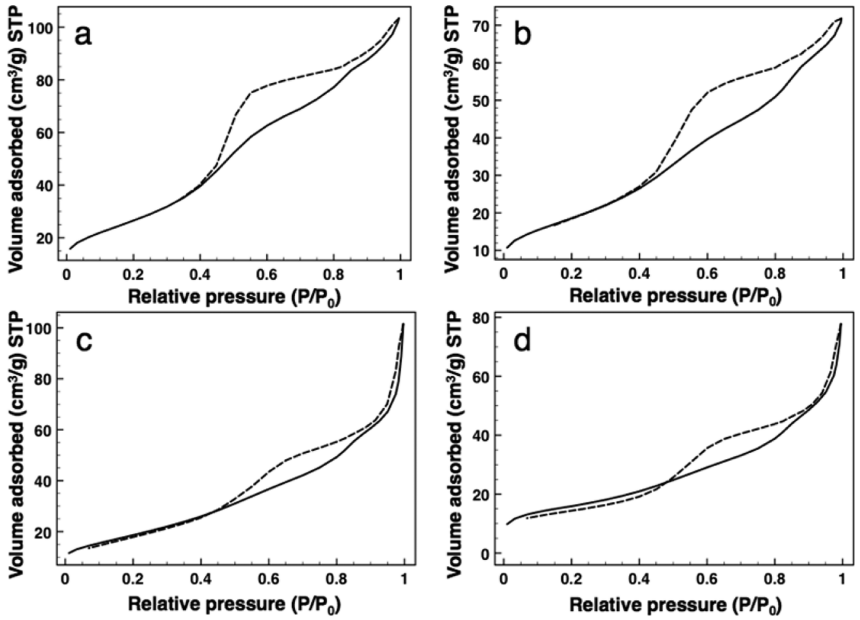

Figure 2. N_2 adsorption−desorption isotherms for (a) *meso*-Co_3O_4, (b) *meso*-Co_3O_4/CeO_2, (c) *meso*-Co_3O_4/10%La-CeO_2, and (d) *meso*-Co_3O_4/10%Mn-CeO_2. Solid lines represent adsorption and dashed lines represent desorption.

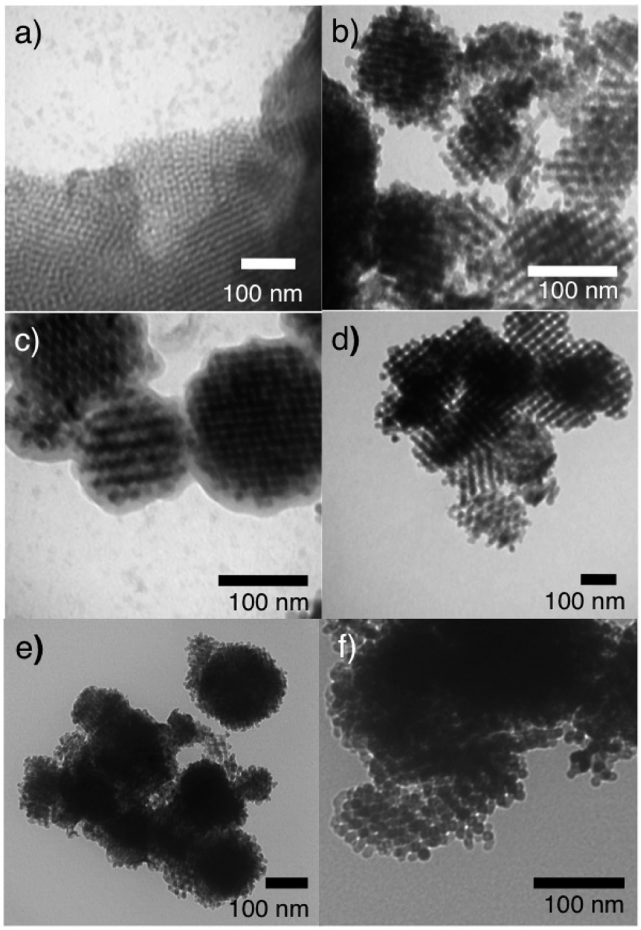

Figure 3. TEM images of (a) KIT-6, (b) *meso*-Co_3O_4, (c) *meso*-Co_3O_4/$Ce(NO_3)_3{\cdot}6H_2O$, (d) *meso*-Co_3O_4/CeO_2, (e) *meso*-Co_3O_4/10%La-CeO_2, and (f) *meso*-Co_3O_4/10%Mn-CeO_2.

materials do not lose their mesoporous structure when some of the pores are filled with doped or undoped CeO_2. Low angle PXRD measurements (Figure S2, Supporting Information) show peaks at low angles for all synthesized materials due to the ordered nature of the mesopores. KIT-6 itself has cubic Ia3d symmetry and this ordered structure is retained in the templated products. The pore size distribution curves of *meso*-Co_3O_4, *meso*-Co_3O_4/CeO_2, *meso*-Co_3O_4/10%La-CeO_2 and *meso*-Co_3O_4/10%Mn-CeO_2 are presented in Figure S3 (Supporting Information). *meso*-Co_3O_4 has an average pore size of 4.4 nm, while *meso*-Co_3O_4/CeO_2, *meso*-Co_3O_4/10%La-CeO_2, and *meso*-Co_3O_4/10%Mn-CeO_2 have pore diameters of 4.8, 7.0, and 7.3 nm, respectively. The doped CeO_2 samples have larger pore sizes and greater pore size distributions, possibly due to the dopant disrupting the CeO_2 lattice structure. Any CeO_2 that does not enter the *meso*-Co_3O_4 forms small particles with pore-like voids between them.

TEM of the samples show that the *meso*-Co_3O_4 inverse KIT-6 morphology is maintained upon removal of the silica template (Figure 3). After addition of $Ce(NO_3)_3{\cdot}6H_2O$ the material is calcined under air for 5 h and again the mesoporous morphology of the *meso*-Co_3O_4 remains intact, with some of the pores filled with CeO_2.

The chemical composition of the new materials was examined by energy dispersive X-ray (EDX) spectroscopy. EDX spectra from *meso*-Co_3O_4 show the elements cobalt and oxygen, with a trace amount of silicon remaining from the KIT-6 template. After the CeO_2 was added, cobalt, oxygen and cerium are all observed by EDX of *meso*-Co_3O_4/CeO_2. Similarly, EDX measurements indicate that cobalt, oxygen, cerium, and lanthanum or manganese are present in *meso*-Co_3O_4/10%La-CeO_2 and *meso*-Co_3O_4/10%Mn-CeO_2, respectively. EDX mapping (Figures S4 and S5, Supporting Information) shows homogeneous dispersion of all elements present, which is expected as the resolution is not high enough to image the individual mesopores.

X-ray photoelectron spectroscopy (XPS) was also used to determine the chemical composition of the materials. Figure 4 shows the high resolution Ce 3d XPS spectra collected from *meso*-Co_3O_4/CeO_2, *meso*-Co_3O_4/10%La-CeO_2 and *meso*-

DOI: 10.1021/acsami.5b02367
ACS Appl. Mater. Interfaces 2015, 7, 11460−11466

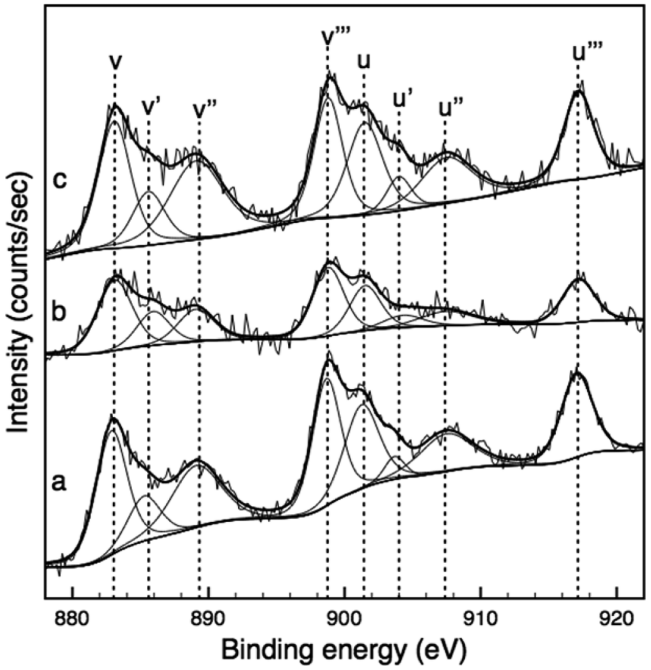

Figure 4. High-resolution Ce 3d XPS spectra of (a) *meso*-Co_3O_4/CeO_2, (b) *meso*-Co_3O_4/10%La-CeO_2, and (c) *meso*-Co_3O_4/10%Mn-CeO_2.

Co_3O_4/10%Mn-CeO_2. Following convention, two sets of multiplets u and v ($3d_{3/2}$ and $3d_{5/2}$ spin−orbit components) have been labeled, with splitting of 18.4 eV, in agreement with the literature.[19,34] Three pairs of peaks denoted as V/U, V″/U″, V‴/U‴ are assigned to Ce^{4+} species and arise from different Ce 4f electron configurations in the final states (Table S2, Supporting Information). The couple V′/U′ is attributed to the electron configuration of the final state of the Ce^{3+} species.[34−36]

The position of the Co $2p_{3/2}$ and $2p_{1/2}$ peaks in the XPS spectra for all samples confirms the presence of Co_3O_4, as illustrated in Figure 5 and Table S3 (Supporting Information).[37,38] An extremely weak satellite structure symptomatic of shakeup from the minor Co^{2+} component can be seen in *meso*-Co_3O_4, but it is completely absent from *meso*-Co_3O_4/CeO_2, *meso*-Co_3O_4/10%La-CeO_2 and *meso*-Co_3O_4/10%Mn-CeO_2.[39,40]

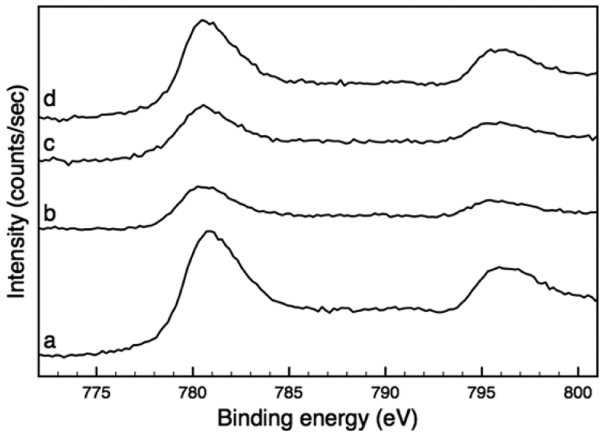

Figure 5. High-resolution Co 2d XPS spectra of (a) *meso*-Co_3O_4, (b) *meso*-Co_3O_4/CeO_2, (c) *meso*-Co_3O_4/10%La-CeO_2, and (d) *meso*-Co_3O_4/10%Mn-CeO_2.

These peaks are not strong enough to be assigned as the shakeup peaks characteristic of the Co^{2+} in CoO and it is likely that they arise from the very small amount of Co^{2+} present in mixed-valence Co_3O_4. XPS data for *meso*-Co_3O_4/10%La-CeO_2 and *meso*-Co_3O_4/10%Mn-CeO_2 also confirms the presence of La and Mn, respectively (Figures S6 and S7, Supporting Information).

All of the materials prepared were investigated for the complete oxidation of methane (Scheme 2) by temperature-

Scheme 2. Total Oxidation of Methane Investigated in This Study

$$CH_4 + 2\,O_2 \longrightarrow CO_2 + 2\,H_2O$$

programmed oxidation (TPO). Interestingly, when tested for catalytic activity for complete methane oxidation, *meso*-Co_3O_4 showed high activity at low temperatures with 50% complete methane conversion ($T_{50\%}$) at 390 °C (Figure 6; compared to

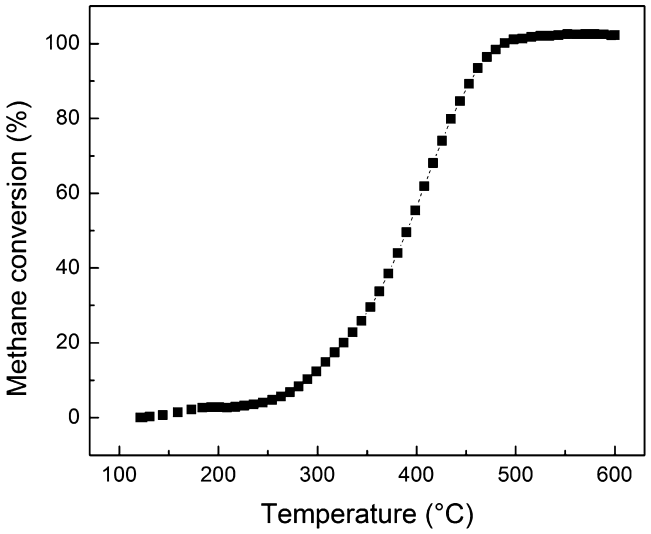

Figure 6. TPO curve of *meso*-Co_3O_4.

$T_{50\%}$ of 250 °C for a conventional precious metal-containing catalyst (7.7 wt % Pd/SiO_2) tested under the same TPO reaction conditions[41]). Although the complete sequence of elementary steps governing hydrocarbon oxidation on metal oxide surfaces is not completely understood, the reaction is thought to occur through C—H activation with a simultaneous reduction of metal oxide surface sites.[15,42] As indicated by the very weak nature of the Co^{2+} satellite peaks in the XPS spectrum, there is almost no Co^{2+} on the surface of the catalysts. Therefore, we propose that Co^{3+} sites on the surface of the *meso*-Co_3O_4 are reduced to Co^{2+} by activation of CH_4, and may generate surface hydroxide ions. This is similar to the mechanism proposed for hydrocarbon oxidation over other metal oxides.[42,43]

meso-Co_3O_4/CeO_2, *meso*-Co_3O_4/10%La-CeO_2, and *meso*-Co_3O_4/10%Mn-CeO_2 show high catalytic activity for materials that do not contain noble metals as seen in Figure 7 and Table 1, with the $T_{50\%}$ at 400 °C for *meso*-Co_3O_4/10%La-CeO_2 and 445 °C for *meso*-Co_3O_4/10%Mn-CeO_2. The weight hourly space velocity (WHSV) of 180,000 mL/g/h is significantly higher than most literature examples of similar catalysts, indicating that the materials described here are much more

DOI: 10.1021/acsami.5b02367
ACS Appl. Mater. Interfaces 2015, 7, 11460−11466

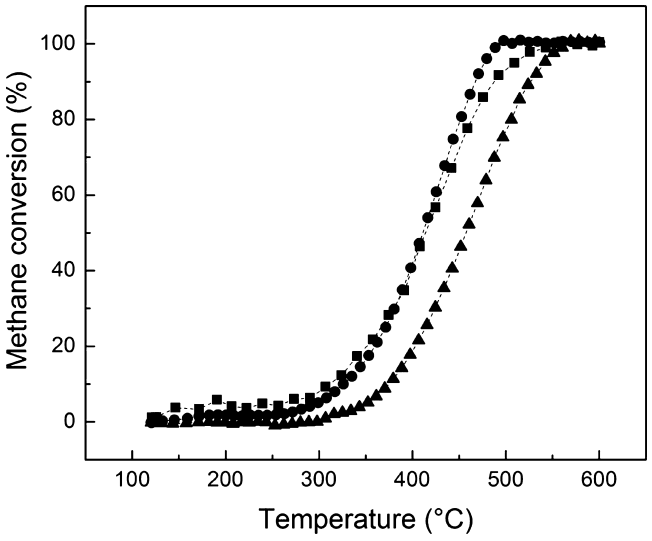

Figure 7. TPO curves for (■) *meso*-Co_3O_4/CeO_2, (●) *meso*-Co_3O_4/10%La-CeO_2, and (▲) *meso*-Co_3O_4/10%Mn-CeO_2.

active for methane oxidation. At 100% conversion, the only products were CO_2 and H_2O. It is probable that the reduction in surface area associated with the addition of CeO_2 or doped CeO_2 causes the slight decrease in catalytic activity. It is also possible that Co_3O_4 catalysts containing CeO_2 have metal−metal interactions between the Co and Ce that alter the redox properties of the materials, with electron transfer between the two metal oxides preventing the reduction of the *meso*-Co_3O_4 surface at low temperatures. Although the introduction of CeO_2 and doped CeO_2 did not have any significant effect on catalytic activity, it is important to note that doping was successful, and the high catalytic activity was maintained. This will allow the catalysts to be more easily modified to increase chances of success in various applications for which methane oxidation is required. These catalytic materials could also act as active supports for noble metals.

CONCLUSIONS

Mesoporous Co_3O_4- and Co_3O_4/CeO_2-based catalysts were prepared by templating with KIT-6 mesoporous silica. Mesostructured Co_3O_4/CeO_2 materials doped with ∼10% manganese and lanthanum were also prepared by a similar procedure. *meso*-Co_3O_4 shows unusually high methane oxidation activity with a light-off temperature of 390 °C. *meso*-Co_3O_4/CeO_2, *meso*-Co_3O_4/10%La-CeO_2, and *meso*-Co_3O_4/10%Mn-CeO_2 show high activity for total oxidation of methane, with light-off temperatures of 407, 400, and 445 °C, respectively. These materials with hierarchical mesoporous structures may be applied for low-temperature methane oxidation and other catalytic reactions.

ASSOCIATED CONTENT

Supporting Information

N_2 adsorption−desorption isotherm, BJH pore size distribution curves, and TEM image of KIT-6. Crystallite sizes, low-angle PXRD, and BJH pore size distribution curves of *meso*-Co_3O_4, *meso*-Co_3O_4/CeO_2, *meso*-Co_3O_4/10%La-CeO_2, and *meso*-Co_3O_4/10%Mn-CeO_2. EDX spectra of *meso*-Co_3O_4/CeO_2, *meso*-Co_3O_4/10%La-CeO_2, and *meso*-Co_3O_4/10%Mn-CeO_2. XPS spectra of *meso*-Co_3O_4/10%La-CeO_2, and *meso*-Co_3O_4/10%Mn-CeO_2. The Supporting Information is available free of charge on the ACS Publications website at DOI: 10.1021/acsami.5b02367.

AUTHOR INFORMATION

Corresponding Authors

*E-mail: mmaclach@chem.ubc.ca
*E-mail: kjs@mail.ubc.ca.

Notes

The authors declare no competing financial interest.

ACKNOWLEDGMENTS

We thank the Natural Sciences and Engineering Research Council (NSERC) of Canada for funding. We are grateful to Dr. K. Wong from UBC for XPS analyses and to S. Munshi at Westport for useful discussions.

REFERENCES

(1) DeLuchi, M. A. *Emissions of Greenhouse Gases from the Use of Transportation Fuels and Electricity*; Argonne National Laboratory: Argonne, IL, 1991.
(2) Lelieveld, J.; Crutzen, P. J. Indirect Chemical Effects of Methane on Climate Warming. *Nature* **1992**, *355*, 339−342.
(3) Gélin, P.; Primet, M. Complete Oxidation of Methane at Low Temperature over Noble Metal Based Catalysts: A Review. *Appl. Catal., B* **2002**, *39*, 1−37.
(4) Cargnello, M.; Delgado Jaén, J. J.; Hernández Garrido, J. C.; Bakhmutsky, K.; Montini, T.; Calvino Gámez, J. J.; Gorte, R. J.; Fornasiero, P. Exceptional Activity for Methane Combustion over Modular Pd@CeO_2 Subunits on Functionalized Al_2O_3. *Science* **2012**, *337*, 713−717.
(5) Sekizawa, K.; Widjaja, H.; Maeda, S.; Ozawa, Y.; Eguchi, K. Low Temperature Oxidation of Methane over Pd Catalyst Supported on Metal Oxides. *Catal. Today* **2000**, *59*, 69−74.
(6) Anderson, R. B.; Stein, K. C.; Feenan, J. J.; Hofer, L. J. E. Catalytic Oxidation of Methane. *Ind. Eng. Chem.* **1961**, *53*, 809−812.
(7) Yao, H. C.; Yu Yao, Y. F. Ceria in Automotive Exhaust Catalysts: I. Oxygen Storage. *J. Catal.* **1984**, *86*, 254−265.

Table 1. Catalytic Performance of the Materials Described in This Paper and Materials from the Literature

composition	preparation method	$T_{50\%}$ (°C)	catalyst mass (mg)	WHSV (mL/g/h)	CH_4 in feed gas (vol %)	ref
meso-Co_3O_4	as described	390	100	180 000	0.1	
meso-Co_3O_4/CeO_2	as described	407	100	180 000	0.1	
meso-Co_3O_4/10%La-CeO_2	as described	400	100	180 000	0.1	
meso-Co_3O_4/10%Mn-CeO_2	as described	445	100	180 000	0.1	
30%Co_3O4−CeO_2	coprecipitation	400	50	12 000	0.3	44
25%Co−Ce−O composite	modified citrate sol−gel method	401	100	30 000	1.0	19
40%La/CeO_2	hydrothermal	<500	100	30 000	1.0	9
$MnCo_2O_4$	fast heating Mn/Co alkoxyacetate precursors	405	200	7020	1.0	45

DOI: 10.1021/acsami.5b02367
ACS Appl. Mater. Interfaces 2015, 7, 11460−11466

(8) Tompos, A.; Margitfalvi, J. L.; Tfirst, E.; Végvári, L.; Jaloull, M. A.; Khalfalla, H. A.; Elgarni, M. M. Development of Catalyst Libraries for Total Oxidation of Methane: A Case Study for Combined Application of "Holographic Research Strategy and Artificial Neural Networks" in Catalyst Library Design. *Appl. Catal., A* **2005**, *285*, 65−78.
(9) Li, H.; Lu, G.; Wang, Y.; Guo, Y.; Guo, Y. Synthesis of Flower-like La or Pr-Doped Mesoporous Ceria Microspheres and Their Catalytic Activities for Methane Combustion. *Catal. Commun.* **2010**, *11*, 946−950.
(10) Li, X.; Ni, C.; Chen, F.; Lu, X.; Chen, Z. Mesoporous Mesocrystal $Ce_{1-x}Zr_xO_2$ with Enhanced Catalytic Property for CO Conversion. *J. Solid State Chem.* **2009**, *182*, 2185−2190.
(11) Shi, L.; Chu, W.; Qu, F.; Luo, S. Low-Temperature Catalytic Combustion of Methane over MnO_x−CeO_2 Mixed Oxide Catalysts: Effect of Preparation Method. *Catal. Lett.* **2007**, *113*, 59−64.
(12) Reddy, B. M.; Bharali, P.; Saikia, P.; Khan, A.; Loridant, S.; Muhler, M.; Grünert, W. Hafnium Doped Ceria Nanocomposite Oxide as a Novel Redox Additive for Three-Way Catalysts. *J. Phys. Chem. C* **2007**, *111*, 1878−1881.
(13) Zhang, Y.; Andersson, S.; Muhammed, M. Nanophase Catalytic Oxides: I. Synthesis of Doped Cerium Oxides as Oxygen Storage Promoters. *Appl. Catal., B* **1995**, *6*, 325−337.
(14) Luo, J. Y.; Meng, M.; Li, X.; Li, X. G.; Zha, Y. Q.; Hu, T. D.; Xie, Y. N.; Zhang, J. Mesoporous Co_3O_4−CeO_2 and Pd/Co_3O_4−CeO_2 Catalysts: Synthesis, Characterization and Mechanistic Study of Their Catalytic Properties for Low-Temperature CO Oxidation. *J. Catal.* **2008**, *254*, 310−324.
(15) Liotta, L. F.; Wu, H.; Pantaleo, G.; Venezia, A. M. Co_3O_4 Nanocrystals and Co_3O_4−MO_x Binary Oxides for CO, CH_4 and VOC Oxidation at Low Temperatures: A Review. *Catal. Sci. Technol.* **2013**, *3*, 3085−3102.
(16) Xue, L.; Zhang, C.; He, H.; Teraoka, Y. Catalytic Decomposition of N_2O over CeO_2 Promoted Co_3O_4 Spinel Catalyst. *Appl. Catal., B* **2007**, *75*, 167−174.
(17) Liotta, L. F.; Ousmane, M.; Di Carlo, G.; Pantaleo, G.; Deganello, G.; Marcì, G.; Retailleau, L.; Giroir-Fendler, A. Total Oxidation of Propene at Low Temperature over Co_3O_4−CeO_2 Mixed Oxides: Role of Surface Oxygen Vacancies and Bulk Oxygen Mobility in the Catalytic Activity. *Appl. Catal., A* **2008**, *347*, 81−88.
(18) Kang, M.; Song, M. W.; Lee, C. H. Catalytic Carbon Monoxide Oxidation over CoO_x/CeO_2 Composite Catalysts. *Appl. Catal., A* **2003**, *251*, 143−156.
(19) Li, H.; Lu, G.; Qiao, D.; Wang, Y.; Guo, Y.; Guo, Y. Catalytic Methane Combustion over Co_3O_4/CeO_2 Composite Oxides Prepared by Modified Citrate Sol−Gel Method. *Catal. Lett.* **2011**, *141*, 452−458.
(20) Liotta, L. F.; Di Carlo, G.; Pantaleo, G.; Venezia, A. M.; Deganello, G. Co_3O_4/CeO_2 Composite Oxides for Methane Emissions Abatement: Relationship between Co_3O_4−CeO_2 Interaction and Catalytic Activity. *Appl. Catal., B* **2006**, *66*, 217−227.
(21) Kleitz, F.; Hei Choi, S.; Ryoo, R. Cubic Ia3d Large Mesoporous Silica: Synthesis and Replication to Platinum Nanowires, Carbon Nanorods and Carbon Nanotubes. *Chem. Commun.* **2003**, 2136−2137.
(22) Yue, W.; Zhou, W. Synthesis of Porous Single Crystals of Metal Oxides via a Solid−Liquid Route. *Chem. Mater.* **2007**, *19*, 2359−2363.
(23) Rossinyol, E.; Arbiol, J.; Peiró, F.; Cornet, A.; Morante, J. R.; Tian, B.; Bo, T.; Zhao, D. Nanostructured Metal Oxides Synthesized by Hard Template Method for Gas Sensing Applications. *Sens. Actuators, B* **2005**, *109*, 57−63.
(24) Jiao, F.; Shaju, K. M.; Bruce, P. G. Synthesis of Nanowire and Mesoporous Low-Temperature $LiCoO_2$ by a Post-Templating Reaction. *Angew. Chem., Int. Ed. Engl.* **2005**, *44*, 6550−6553.
(25) Yue, W.; Zhou, W. Porous Crystals of Cubic Metal Oxides Templated by Cage-Containing Mesoporous Silica. *J. Mater. Chem.* **2007**, *17*, 4947−4952.
(26) Ren, Y.; Ma, Z.; Qian, L.; Dai, S.; He, H.; Bruce, P. G. Ordered Crystalline Mesoporous Oxides as Catalysts for CO Oxidation. *Catal. Lett.* **2009**, *131*, 146−154.
(27) Tüysüz, H.; Comotti, M.; Schüth, F. Ordered Mesoporous Co_3O_4 as Highly Active Catalyst for Low Temperature CO-Oxidation. *Chem. Commun.* **2008**, 4022−4024.
(28) Garcia, T.; Agouram, S.; Sánchez-Royo, J. F.; Murillo, R.; Mastral, A. M.; Aranda, A.; Vázquez, I.; Dejoz, A.; Solsona, B. Deep Oxidation of Volatile Organic Compounds Using Ordered Cobalt Oxides Prepared by a Nanocasting Route. *Appl. Catal., A* **2010**, *386*, 16−27.
(29) Du, Y.; Meng, Q.; Wang, J.; Yan, J.; Fan, H.; Liu, Y.; Dai, H. Three-Dimensional Mesoporous Manganese Oxides and Cobalt Oxides: High-Efficiency Catalysts for the Removal of Toluene and Carbon Monoxide. *Microporous Mesoporous Mater.* **2012**, *162*, 199−206.
(30) Ma, C. Y.; Mu, Z.; Li, J. J.; Jin, Y. G.; Cheng, J.; Lu, G. Q.; Hao, Z. P.; Qiao, S. Z. Mesoporous Co_3O_4 and Au/Co_3O_4 Catalysts for Low-Temperature Oxidation of Trace Ethylene. *J. Am. Chem. Soc.* **2010**, *132*, 2608−2613.
(31) Yue, W.; Hill, A. H.; Harrison, A.; Zhou, W. Mesoporous Single-Crystal Co_3O_4 Templated by Cage-Containing Mesoporous Silica. *Chem. Commun.* **2007**, 2518−2520.
(32) Pereira, G. J.; Castro, R. H. R.; de Florio, D. Z.; Muccillo, E. N. S.; Gouvêa, D. Densification and Electrical Conductivity of Fast Fired Manganese-Doped Ceria Ceramics. *Mater. Lett.* **2005**, *59*, 1195−1199.
(33) Sing, K. S. W.; Everett, D. H.; Haul, R. A. W.; Moscou, L.; Pierotti, R. A.; Rouquérol, J.; Siemieniewska, T. Reporting Physisorption Data for Gas/solid Systems with Special Reference to the Determination of Surface Area and Porosity (Recommendations 1984). *Pure Appl. Chem.* **1985**, *57*, 603−619.
(34) Alexandrou, M.; Nix, R. M. The Growth, Structure and Stability of Ceria Overlayers on Pd(111). *Surf. Sci.* **1994**, *321*, 47−57.
(35) Burroughs, P.; Hamnett, A.; Orchard, A. F.; Thornton, G. Satellite Structure in the X-Ray Photoelectron Spectra of Some Binary and Mixed Oxides of Lanthanum and Cerium. *J. Chem. Soc., Dalt. Trans.* **1976**, 1686−1698.
(36) Bera, P.; Anandan, C. XRD and XPS Studies of Room Temperature Spontaneous Interfacial Reaction of CeO_2 Thin Films on Si and Si_3N_4 Substrates. *RSC Adv.* **2014**, *4*, 62935−62939.
(37) McIntyre, N. S.; Cook, M. G. X-Ray Photoelectron Studies on Some Oxides and Hydroxides of Cobalt, Nickel, and Copper. *Anal. Chem.* **1975**, *47*, 2208−2213.
(38) Garbowski, E.; Guenin, M.; Marion, M.-C.; Primet, M. Catalytic Properties and Surface States of Cobalt-Containing Oxidation Catalysts. *Appl. Catal.* **1990**, *64*, 209−224.
(39) Xu, R.; Wang, J.; Li, Q.; Sun, G.; Wang, E.; Li, S.; Gu, J.; Ju, M. Porous Cobalt Oxide (Co_3O_4) Nanorods: Facile Syntheses, Optical Property and Application in Lithium-Ion Batteries. *J. Solid State Chem.* **2009**, *182*, 3177−3182.
(40) Chuang, T. J.; Brundle, C. R.; Rice, D. W. Interpretation of the X-Ray Photoemission Spectra of Cobalt Oxides and Cobalt Oxide Surfaces. *Surf. Sci.* **1976**, *59*, 413−429.
(41) Gholami, R.; Smith, K. J. Activity of PdO/SiO_2 Catalysts for CH_4 Oxidation Following Thermal Treatments. *Appl. Catal., B* **2015**, *168*−*169*, 156−163.
(42) Baldi, M.; Escribano, V. S.; Amores, J. M. G.; Milella, F.; Busca, G. Characterization of Manganese and Iron Oxides as Combustion Catalysts for Propane and Propene. *Appl. Catal., B* **1998**, *17*, L175−L182.
(43) Wang, Y.; Yang, X.; Hu, L.; Li, Y.; Li, J. Theoretical Study of the Crystal Plane Effect and Ion-Pair Active Center for C−H Bond Activation by Co_3O_4 Nanocrystals. *Chin. J. Catal.* **2014**, *35*, 462−467.
(44) Liotta, L. F.; Di Carlo, G.; Pantaleo, G.; Deganello, G. Co_3O_4/CeO_2 and Co_3O_4/CeO_2−ZrO_2 Composite Catalysts for Methane Combustion: Correlation between Morphology Reduction Properties and Catalytic Activity. *Catal. Commun.* **2005**, *6*, 329−336.
(45) Liu, L.; Zhang, X.; Liu, J. Facile Synthesis of Mn−Co Oxide Nanospheres with Controllable Interior Structures and Their Catalytic Properties for Methane Combustion. *Mater. Lett.* **2014**, *136*, 209−213.

DOI: 10.1021/acsami.5b02367
ACS Appl. Mater. Interfaces 2015, 7, 11460−11466